OXFORD

ORIGINAL ARTICLE

TWEAK/Fn14, a pathway and novel therapeutic target in myotonic dystrophy

Ramesh S. Yadava[1,†], Erin P. Foff[2,†], Qing Yu[1], Jordan T. Gladman[1], Yun K. Kim[1], Kirti S. Bhatt[3], Charles A. Thornton[3], Timothy S. Zheng[4] and Mani S. Mahadevan[1,*]

[1]Department of Pathology and [2]Department of Neurology, University of Virginia, Charlottesville, VA 22908, USA, [3]Department of Neurology, University of Rochester, Rochester, NY 14642, USA and [4]Department of Immunology, Biogen Idec, Cambridge, MA 02142, USA

*To whom correspondence should be addressed at: Mani S. Mahadevan, 415 Lane Rd, MR5 Rm 3330, Charlottesville, VA 22908, USA. Tel: +1 4342434816; Fax: +1 4349241545; Email: mahadevan@virginia.edu

Abstract

Myotonic dystrophy type 1 (DM1), the most prevalent muscular dystrophy in adults, is characterized by progressive muscle wasting and multi-systemic complications. DM1 is the prototype for disorders caused by RNA toxicity. Currently, no therapies exist. Here, we identify that fibroblast growth factor-inducible 14 (Fn14), a member of the tumor necrosis factor receptor super-family, is induced in skeletal muscles and hearts of mouse models of RNA toxicity and in tissues from DM1 patients, and that its expression correlates with severity of muscle pathology. This is associated with downstream signaling through the NF-κB pathways. In mice with RNA toxicity, genetic deletion of *Fn14* results in reduced muscle pathology and better function. Importantly, blocking TWEAK/Fn14 signaling with an anti-TWEAK antibody likewise improves muscle histopathology and functional outcomes in affected mice. These results reveal new avenues for therapeutic development and provide proof of concept for a novel therapeutic target for which clinically available therapy exists to potentially treat muscular dystrophy in DM1.

Introduction

Muscular dystrophies are a heterogeneous group of inherited disorders that result in progressive, devastating muscle damage and functional disability. Myotonic dystrophy type 1 (DM1) is the most common in adults and currently there is no treatment (1). Though it has been over two decades since the DM1 mutation was discovered, the molecular basis of muscular dystrophy in DM1 is still obscure. DM1 is caused by a $(CTG)_n$ expansion in the 3′ untranslated region (3′UTR) of the DM protein kinase (*DMPK*) gene resulting in expression of a toxic RNA which accumulates in the nuclei of affected cells (2–4). Substantial evidence exists for RNA toxicity as the root cause in DM1 (2,5,6). The $(CUG)_n$

expanded RNAs are thought to sequester and/or alter the functional levels of RNA-binding proteins, including members of the Muscleblind-like (MBNL1) and CUG-BP and ETR-3 like factor families, leading to aberrant splicing of numerous other RNAs and the resultant phenotypes (7). Therapeutic developments have primarily focused on targeting the toxic RNA or affecting its interactions with MBNL1 (8–10). However, growing evidence suggests that RNA toxicity has far reaching consequences beyond splicing defects (11–14).

In the course of investigating additional mechanisms of RNA toxicity in DM1, we discovered that fibroblast growth factor-inducible 14 (Fn14) is significantly induced in skeletal and cardiac

---

muscles. Fn14, the smallest member of the tumor necrosis factor receptor super-family ([15]) binds TWEAK (tumor necrosis factor-like weak inducer of apoptosis) a type II transmembrane protein ([16],[17]). Here, we show for the first time, the adverse effects of increased Fn14 and TWEAK/Fn14 signaling on muscle function and pathology using mouse models of RNA toxicity in DM1. In addition, we demonstrate the potential benefits of a novel, clinically available therapy specifically targeting the TWEAK/Fn14 pathway.

Results

Fn14 is induced by RNA toxicity in DM1

Previously, we developed the first inducible/reversible mouse models of RNA toxicity in DM1 (termed DM5) in which over-expression of an eGFP-*DMPK* 3′UTR (CUG)$_5$ mRNA results in cardinal features of DM1 including cardiac conduction defects, myotonia, abnormal muscle pathology and RNA splicing deficits ([5]). To identify novel mechanisms of RNA toxicity, we exploited the potential to induce and reverse the disease process at will. Using microarray expression analyses, we discovered that levels of *Fn14* mRNA were highly responsive to the toxic RNA in both heart and skeletal muscles. This was confirmed by northern blotting (Fig. 1A and B), western blotting (Fig. 1C), immunofluorescence (Fig. 1D) and quantitative RT-PCR (qRT-PCR) (Fig. 1E and F). In all the assays, *Fn14* expression was low in uninduced tissues. Immunofluorescence detected specific, sacrolemmal expression of Fn14 expression in DM5 mice with RNA toxicity [DM5-(D+)] (Fig. 1D, Supplementary Material, Fig. S1). Notably, we found no significant differences in the expression of *Tweak* that correlated with the expression of the toxic RNA, in either the heart or skeletal muscles of these mice (Fig. 1G and H). Additionally, qRT-PCR showed that eGFP mRNA expression in DM5-(D+) mice is induced markedly (9-fold) by 2 days and that *Fn14* is up-regulated (2.5-fold) as early as 4 days after induction (Fig. 1I), well before the onset of significant muscle pathology or detectable decline in muscle function. Using a grading scale developed to assess clinical histopathology in skeletal muscles (Supplementary Material, Table S1), we found a clear correlation between the levels of *Fn14* expression and severity of muscle pathology ($P < = 0.01$, Fig. 1J). Importantly, we also found *Fn14* up-regulated in skeletal muscles of an inducible eGFP-*DMPK*-3′ UTR (CTG)$_{200}$ mouse model (termed DM200) ($P < = 0.01$, Fig. 2A and B) and in their hearts (Fig. 2C and D). We also measured *Fn14* expression by RT-PCR in additional mouse models including: (1) mice that have myotonia (*Clcn1$^{-/-}$*), (2) a model of Duchenne muscular dystrophy (*Mdx*), (3) mice that over-express eGFP and (4) the HSA-LR mouse model which over-expresses an RNA with (CUG)$_{250}$ ([6]); and found no notable up-regulation of *Fn14* expression except in the case of mice that over-express the *DMPK* 3′UTR (Supplementary Material, Fig. S2A).

To investigate its clinical relevance, we evaluated *FN14* mRNA, and Fn14 protein expression in muscle samples with mild ($n = 4$) and severe ($n = 4$) histopathology (Supplementary Material, Fig. S2C) from individuals with DM1, and muscles from unaffected individuals ($n = 8$). Both Fn14 mRNA and protein levels were elevated (>10-fold) in severely affected muscles and as in the mice, we found significant up-regulation of Fn14 that correlated with the severity of DM1 histopathology ($P = 0.001$, Fig. 2E and F, Supplementary Material, Fig. S2B). We also found increased Fn14 in DM1 afflicted heart tissues (Fig. 2G and H). As observed in the mouse models, we saw no up-regulation of *TWEAK*.

Furthermore, we studied *FN14* mRNA expression in a collection of tibialis anterior (TA) muscle biopsies obtained from a cohort of unaffected individuals ($n = 11$) and individuals with DM1 ($n = 20$) who had undergone rigorous clinical evaluations including manual muscle strength assessments. We found a clear correlation between the presence of clinical weakness and the level of *FN14* expression in individuals with DM1 ($P = 0.002$) (Fig. 2I). Those with DM1 who were not clinically weak had normal *FN14* mRNA levels whereas the vast majority of those with clinical weakness had elevated *FN14* expression, which on average was about four times greater.

Fn14 deficiency is beneficial in RNA toxicity

Fn14$^{-/-}$ mice are viable, healthy, fertile, and display no overt systemic or muscle-specific phenotypes ([18],[19]). Absence of Fn14 was confirmed by immunofluorescence and western blotting (Supplementary Material, Fig. S3A and B). To clearly evaluate the role of Fn14 in RNA toxicity, these were bred with DM5 homozygotes to obtain homozygous DM5/*Fn14$^{-/-}$* mice, as well as a control group of DM5/*Fn14$^{+/+}$*mice in the appropriate mixed genetic background. We obtained baseline functional data by electromyography (EMG), electrocardiography (ECG), treadmill running and forelimb grip strength on all mice prior to doxycycline administration (D−) and found no significant differences between the two groups. After doxycycline administration (D+), mice were reevaluated at 1 week and 2 weeks post-induction of RNA toxicity. We confirmed by qRT-PCR that toxic RNA levels were equivalent between study groups (Supplementary Material, Fig. S3C). No differences in EMG and ECG studies were observed with all tested mice developing similar degrees of myotonia and cardiac conduction abnormalities at 2 weeks post-induction. However, it was noted that RNA toxicity mice lacking Fn14 seemed to live longer ($P = 0.05$, Mantel–Cox test). Typically DM5-(D+) mice started dying ∼14 days (11 of 21 dead) and only two were alive by 18 days (19 of 21 dead). In contrast, only two mice died by 14 days in the DM5/*Fn14$^{-/-}$*-(D+) group and eight were still alive at 18 days. In addition, these mice had significantly better forelimb grip strength ($P = 0.04$) and treadmill run fitness ($P = 0.01$) (Fig. 3A and B). We also observed remarkable preservation of muscle architecture in the mice lacking Fn14, as compared with the significant damage observed in DM5-(D+) mice (Fig. 3C and Supplementary Material, Fig. S3D). This occurred without any obvious correction of the splicing defects present in these mice (Supplemental Material Fig. S4 and Table S2)

RNA toxicity, TWEAK/Fn14 and NF-κB

We then investigated the intracellular pathways activated in skeletal muscles by TWEAK/Fn14 in both our mouse models of DM1 and in tissues from individuals with DM1. Among other things, stimulation of the TWEAK/Fn14 pathway leads to activation of both the canonical and non-canonical NF-κB signaling pathways ([20–22]). It is thought that signaling through Fn14 results in receptor trimerization, recruitment of TRAF2/cIAP1 (tumor necrosis factor receptor associated factor 2/cellular inhibitors of apoptosis 1) complexes to the receptor, degradation of cIAP1 (BIRC2), and subsequent stabilization of NIK (NF-κB inducing kinase) and signaling through the Iκκ (I kappa B kinase) complexes resulting in activation of both the canonical (p65) and non-canonical (p100/p52) NF-κB pathways (schema, Fig. 4 and Supplementary Material, Figs. S5–6) ([23–27]). No previous work has been done to see if this pathway for TWEAK/Fn14 signaling holds true in human skeletal muscles.
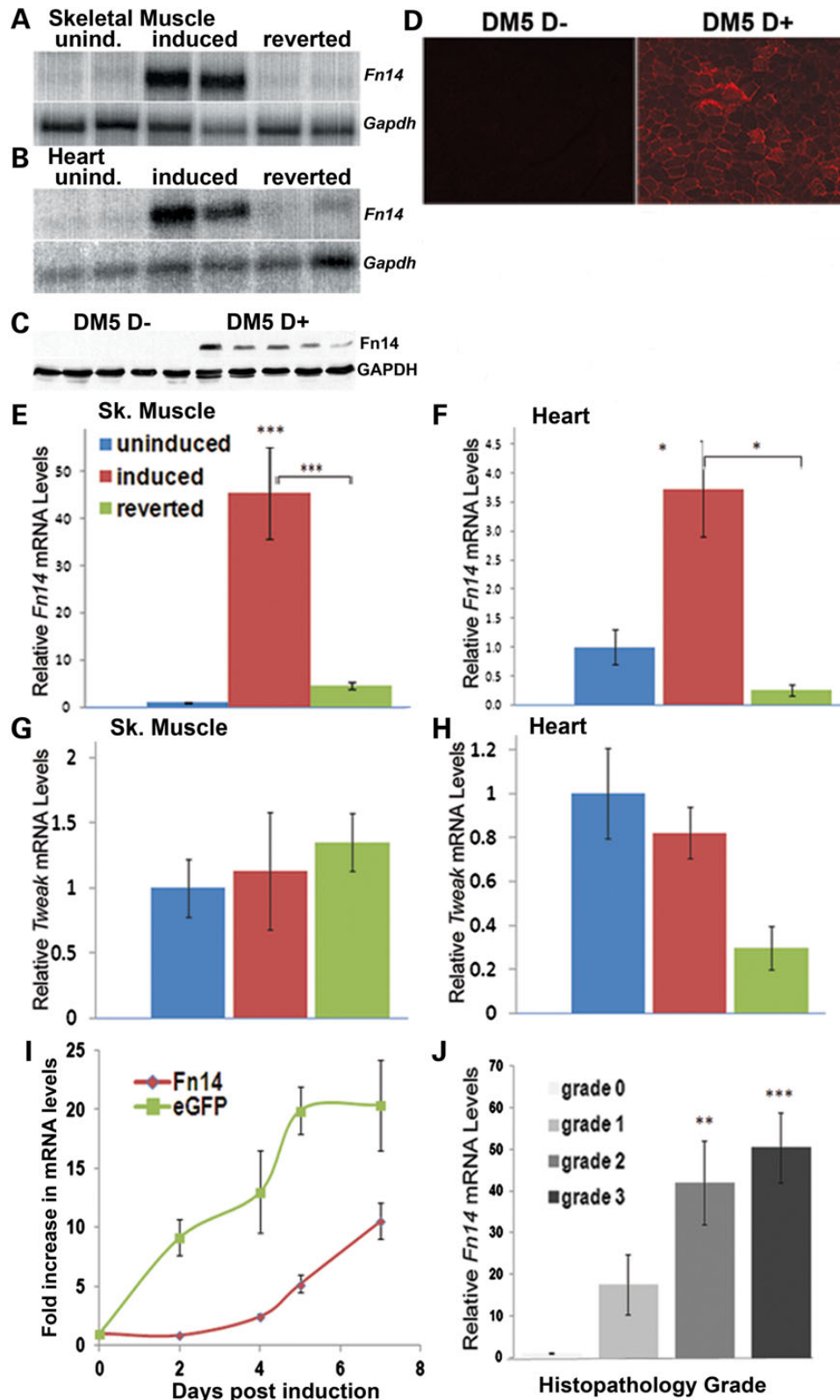
Figure 1. *Fn14* is induced by *DMPK* 3′UTR mRNA toxicity. (**A** and **B**) Northern blots show *Fn14* expression is responsive to RNA toxicity in mouse skeletal muscle and heart. *Gapdh*, loading control. (**C**) Western blot shows increased Fn14 in skeletal muscle of DM5-(D+) mice. (**D**) Immunofluorescence demonstrates high sarcolemmal Fn14 expression (red) in DM5-(D+) mice (see also Supplementary Material, Fig. S1). (**E**) qRT-PCR of *Fn14* expression in skeletal muscle is significantly different between uninduced and induced mice ($P = 0.001$) and induced and reverted mice ($P = 0.003$). (**F**) Similar results are seen in the heart ($P = 0.029$ and $P = 0.016$, respectively) (*$P < 0.05$, ***$P \leq 0.005$). (**G** and **H**) No significant differences were observed with *Tweak* mRNA; ($n \geq 5$ per group for E–H). (**I**) qRT-PCR shows time course for induction of toxic RNA (eGFP) and *Fn14* mRNA in skeletal muscles; ($n = 3$ per group). (**J**) *Fn14* mRNA levels are correlated with muscle histopathology grades in the DM5 mouse model (**$P = 0.01$, ***$P = 0.0009$); ($n = 4$ to 10 per group). For all graphs, errors bars are mean ± SEM Student's *t* test applied to all comparisons.

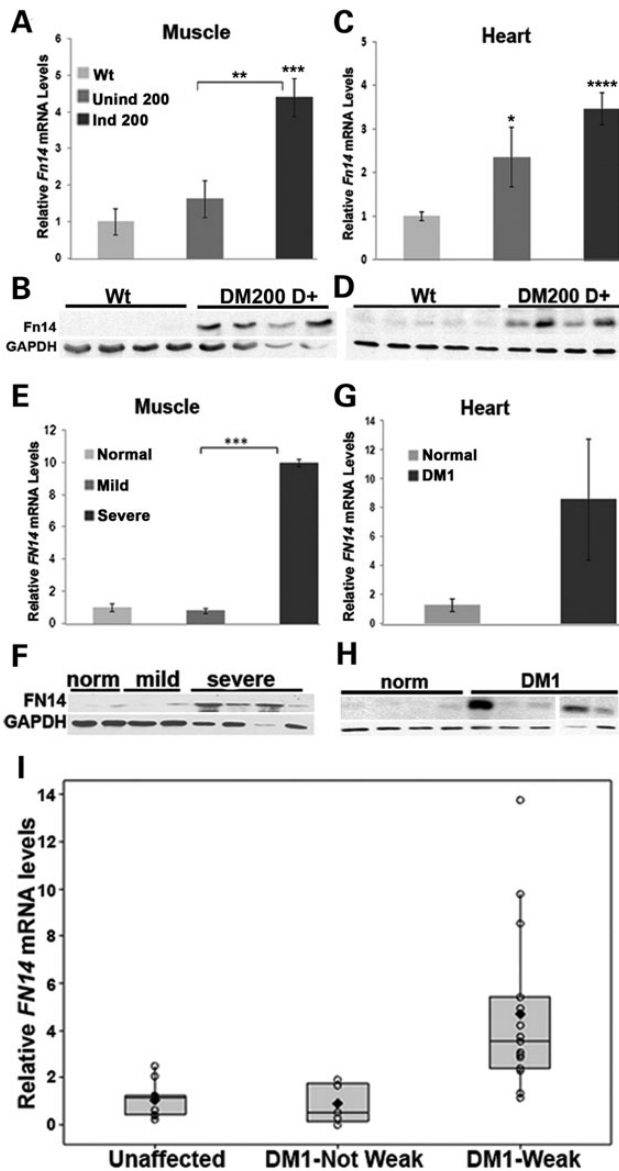**Figure 2.** Fn14 is induced in the DM200 mouse model and in tissues from DM1 patients. (**A–D**) qRT-PCR and western blots show increased *Fn14* mRNA and Fn14 expression in skeletal muscles (A and B) and hearts (C and D) of an inducible *DMPK*-3′UTR (CTG)$_{200}$ mouse model (*$P = 0.04$, **$P = 0.01$, ***$P = 0.002$, ****$P = 0.0001$); ($n = 6$ to 21 per group). (**E** and **F**) qRT-PCR and western blots show increased *FN14* mRNA and Fn14 in human skeletal muscle tissues correlating with severity of DM1 muscle pathology) ($n = 4$ per group), (***$P = 0.001$). (**G** and **H**) Similar results are seen in DM1 affected hearts; (normal, $n = 4$), (DM1, $n = 6$) ($P = 0.06$). Errors bars are mean ± SEM for all graphs. Student's *t* test for all preceding graphs. (**I**) Clinical weakness (as assessed by the MRC-UK manual muscle strength scale) correlates with increased *FN14* mRNA expression ($P = 0.002$; ANOVA); [unaffected ($n = 11$), DM1-not weak ($n = 5$) and DM1-weak ($n = 15$)]. Gray box represents median ± 25% for each group; median represented by line through each gray box; dark diamonds represent mean; open circles represent individual data points; vertical line for each data set represents range of data used in statistical analysis.

Western blotting of protein extracts showed Fn14 is clearly increased in the DM5-(D+) mice and in the severely affected DM1 tissues (Fig. 4A and F). Western blotting showed increased degradation of cIAP1 in DM5-(D+) mice and in the severely affected DM1 tissues (Fig. 4B and G, Supplementary Material, Fig. S7). This coincided with increased NIK expression in skeletal muscles

of DM5-(D+) mice as detected by immunofluorescence (Fig. 4C). Normally NIK levels are kept very low (see DM5-(D−) mice (Fig. 4C)), being tightly regulated through ubiquitination by cIAP1. Immunofluorescence using consecutive tissue sections revealed that increased NIK was associated with increased NF-κB2 (p100/p52) in the same, corresponding muscle fibers (Fig. 4C and Supplementary Material, Fig. S8). Western blotting showed increased processing of p100 to the active p52 form in DM5-(D+) mice (Fig. 4D) and in severely affected DM1 tissues (Fig. 4H and I). Additionally, we noted increased phosphorylated p65 (p-p65) in DM5-(D+) mice and in DM1 tissues (Fig. 4E and J), indicating activation of the canonical NF-κB pathway. Increased Fn14, p-p65 and expression of *Nfkb2* were also noted in the DM200-(D+) mice (Supplementary Material, Fig. S9A–E). In addition, in the cohort of DM1 individuals with detailed clinical assessment, we found significantly increased expression of *NFKB2* in the TA biopsies as compared with those from unaffected individuals (Supplementary Material, Fig. S9F).

To clearly delineate the contribution of Fn14 in the activation of the NF-κB pathway in RNA toxicity, we studied skeletal muscles from DM5/*Fn14*$^{−/−}$-(D+) mice. The increase in p-p65, increased degradation of BIRC2, increased expression of NF-κB2 and increased processing of p100–p52 observed in DM5-(D+) mice were all significantly attenuated by Fn14 deficiency (Fig. 5A–E, Supplementary Material, Fig. S7). qRT-PCR for key components of the NF-κB pathway [*Nfkb2* (p100/p52)], *Nfkb1* (p105/p50), *RelB* and *Map3k14* (NIK) showed significantly increased gene expression of all of them in DM5-(D+) mice (Fig. 5F–I) and showed significant increases in *Nfkb2* mRNA in the DM200-(D+) mice that correlated with levels of *Fn14* expression (Supplementary Material, Fig. S9C–D). In the Fn14 deficient mice, we noted significant attenuation of the effects on *Nfkb2* and *Map3k14* (Fig. 5F and I).

Our preceding analyses were based on the fact that most work on NF-κB over the past decades has focused on expression and effects on the proteins. However, DM1 pathogenesis is primarily focused on RNA splicing defects. There is scant information with regard to alternative splicing of NF-κB components and the resulting biological consequences (28). Nevertheless, we evaluated a number of the reported splicing events that were related to the genes we studied (Supplementary Material, Table S2). Of these, only the exclusion of exon 5 in *RelB*, and exon 22 in *Nfkb1* showed any difference in mice with RNA toxicity, and only exon 22 of *Nfkb1* showed any additional difference due to Fn14 deficiency (Supplementary Material, Fig. S10).

A number of additional mechanisms have been previously invoked in DM1 including defects in regeneration, autophagy, inflammatory pathways, increased ubiquitin proteasome activity and activation of signaling pathways including increased PKC and GSK-3β activity (12). Tweak/Fn14 signaling in skeletal muscle downstream of NFκB has been implicated in a number of pathways including inflammation, metabolism, autophagy and regeneration as well (29). In evaluating the role of Fn14 in the DM5-(D+) mice in some of these pathways, we found evidence for potential beneficial effects of Fn14 deficiency with respect to muscle regeneration (*Myh8*), autophagy (*Maplc3a* and *Maplc3b*), inflammation (*Ccl-2* and *Ccl21a*) and muscle metabolism [*Ppargc1a* (i.e. *Pgc1-α*) and *Ppargc1b* (i.e. *Pgc1-β*)] (Fig. 6A–G). This was reinforced by the fact that we observed decreased expression of *Ccl2* and *Nfkb2* and increased expression of *Ppargc1a* in the hearts of DM5/*Fn14*$^{−/−}$-(D+) mice as compared with the DM5-(D+) mice (Supplementary Material, Fig. S11).

More recently, we have begun studying the role of Fn14 induction in regenerative defects in the skeletal muscles of mice with
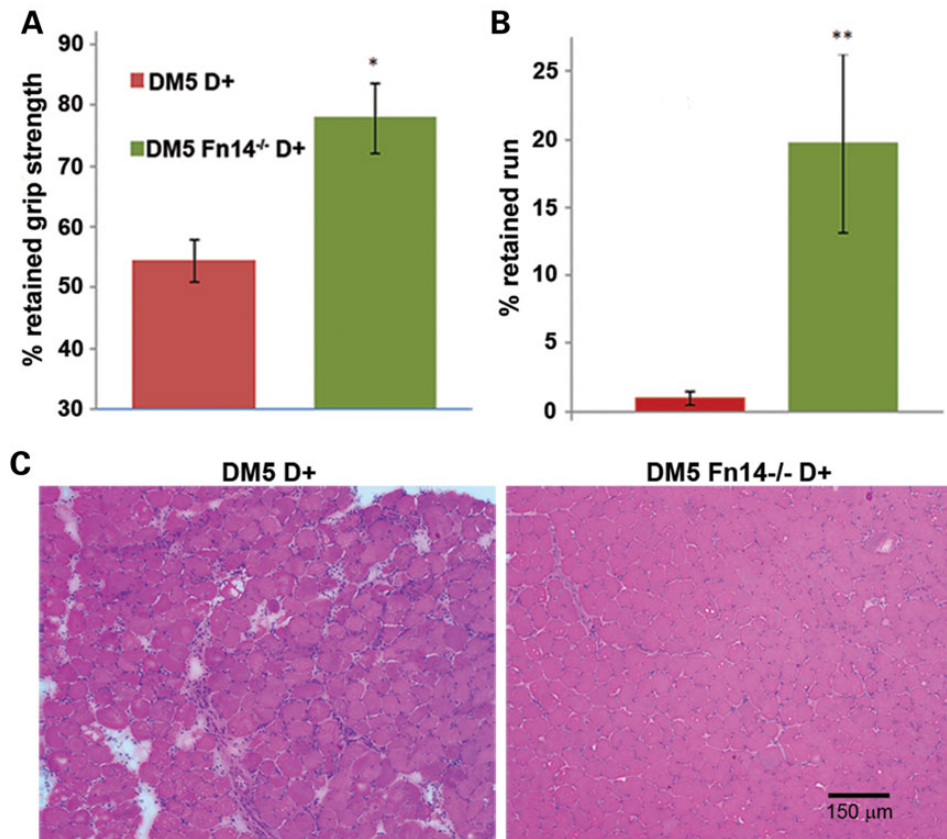
Figure 3. Deletion of Fn14 leads to improved function and muscle histopathology. (**A** and **B**) At 14 days post-induction, improvements in forelimb grip strength (*P = 0.042) and treadmill running distances (**P = 0.013) were noted in DM5-(D+) mice with *Fn14* loss (DM5-(D+) (*n* = 8), DM5*Fn14*$^{-/-}$-(D+) (*n* = 14)). Errors bars are mean ± SEM (Student's *t* test). (**C**) H&E staining of skeletal muscle shows marked improvement in muscle architecture and reduced muscle degeneration in DM5*Fn14*$^{-/-}$-(D+) mice.

RNA toxicity. To study this in a controlled manner that could be compared with others' work ([30](#)), we utilized a widely used and characterized cardiotoxin (CTX) induced muscle injury model which results in inflammation and myofiber degeneration that is followed by muscle regeneration. Skeletal muscle regeneration depends upon muscle precursor cells known as satellite cells that respond to damage and differentiate into myoblasts that fuse to regenerate muscle fibers. PAX7, a transcription factor, is commonly used as a marker of satellite cells using immunofluorescence. Previous work from our laboratory ([31](#)) has found that in non-damaged TA muscle of DM5-(D−) mice, there were approximately three PAX7+ve nuclei per 100 muscle fibers and that the number of PAX7+ve nuclei rose to ∼27 per 100 fibers in skeletal muscle 5 days after CTX damage, at a time when satellite cell and recently committed myoblast number is at its peak ([32](#)). We examined PAX7 expression in the skeletal muscles of DM5-(D+) mice and DM5/*Fn14*$^{-/-}$-(D+) mice that were induced for 7 days and then injected with CTX in their TA muscles. Five days after damage, we found that the number of PAX7+ve nuclei in DM5-(D+) mice was only 13 per 100 fibers, whereas in the DM5/*Fn14*$^{-/-}$-(D+) mice it was 23 nuclei per 100 fibers (P = 0.02, Mann–Whitney) (Fig. [7](#)). This data clearly show that RNA toxicity results in a defect in satellite cell response to damage and that Fn14 deficiency leads to a corrective response.

Therapy targeting TWEAK/Fn14 in RNA toxicity

The preceding experiments clearly demonstrate the potential therapeutic benefits of targeting Fn14 in RNA toxicity associated with DM1, with *Fn14* deletion showing clear beneficial effects. Since Fn14 is increased in individuals with DM1 (Fig. [2](#)F and H), a therapy blocking Fn14 would be ideal. Unfortunately, current anti-Fn14 antibodies seem instead to have an agonistic effect (i.e. mimic TWEAK signaling) and lead to increased cell death in tumor models (US Patent-20090324602A1). TWEAK independent, Fn14 self-activation at high levels of Fn14 expression has been proposed ([18](#)), and it could be possible that anti-Fn14 antibodies are causing receptor trimerization and downstream signaling, independent of the ligand. Anti-TWEAK antibodies are another potential option and have demonstrated benefits in inflammatory diseases such as lupus nephritis and are currently in Phase II clinical trials for this indication ([33](#)).

So, we studied a mouse monoclonal anti-TWEAK antibody, P2D10, as a potential therapy ([25](#)). Age and sex-matched groups of twenty homozygous DM5 adult mice were pre-dosed with intraperitoneal anti-TWEAK (P2D10) (30 μg/g), an isotype control (P1.17) (30 μg/g), or PBS two days prior to induction of toxic RNA, and then dosed every 3 days for the duration of the experiment. Phenotypic testing was performed pre-exposure, and at 1 and 2 weeks post-induction of RNA toxicity, and then mice were euthanized and various tissues collected for subsequent molecular analyses. Using an antibody targeted against the specific IgG isotype of the treatment antibodies (IgG2a), we confirmed the presence of P2D10 and P1.17 in skeletal muscles of treated mice (Fig. [8](#)A and Supplementary Material, Fig. S12B). After 2 weeks of treatment (5 doses of therapy), no obvious differences in the degree of myotonia or cardiac conduction defects were seen. But, we did note a striking preservation of skeletal
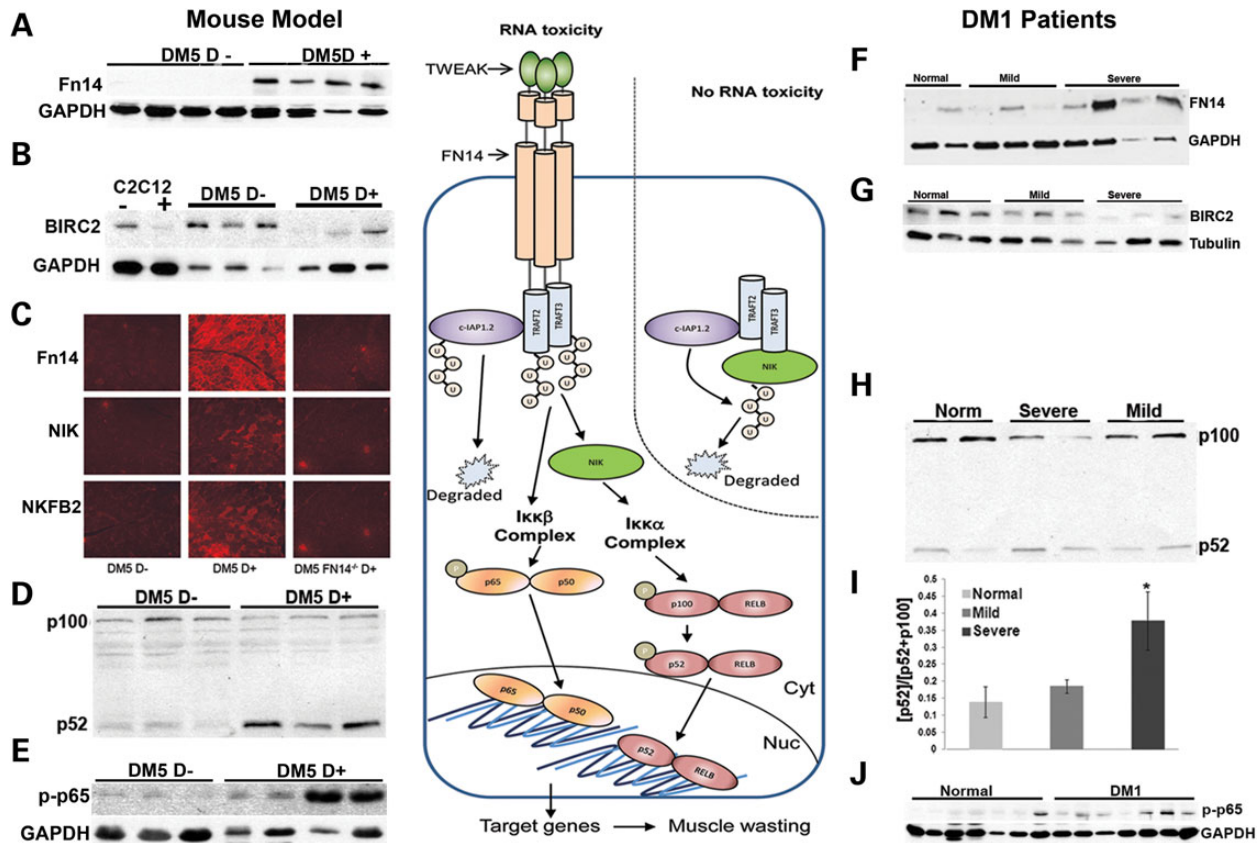
Figure 4. RNA toxicity leads to activation of NF-κB pathway. Schema represents the pathway for TWEAK/Fn14 signaling through NF-κB. (**A** and **B**) Western blots of mouse skeletal muscle protein extracts show increased Fn14 (A), and decreased cIAP1 (BIRC2) in DM5-(D+) (induced) mice (B). (**C**) Immunofluorescence of serial sections shows increased Fn14, NIK and NF-κB2 in skeletal muscle from DM5-(D+) mice and absence of increased NIK or NF-κB2 in DM5$Fn14^{-/-}$-(D+) mice. (**D** and **E**) Western blots show DM5-(D+) mice have increased NF-κB2 p100 processing to p52 (D), and elevated p-p65 (E). (**F–J**) In individuals with DM1, western blotting of skeletal muscle protein extracts show increased Fn14 (F), decreased cIAP1 (BIRC2) (G), increased processing of NF-κB2 p100 to p52 (H), which is quantified in (I); ($n = 4$ per group); error bars are mean ± SEM; *$P = 0.037$ (Student's *t* test); and increased p-p65 in DM1 (J).
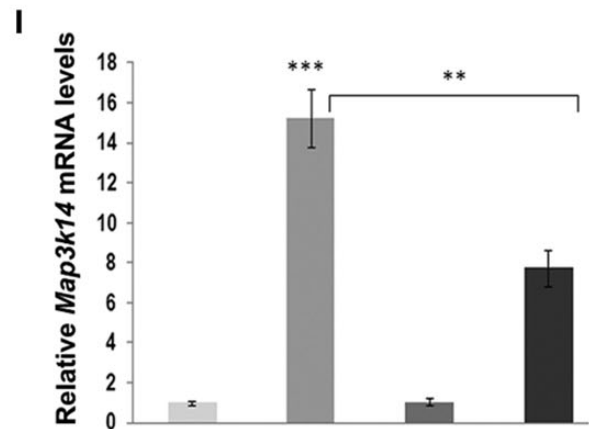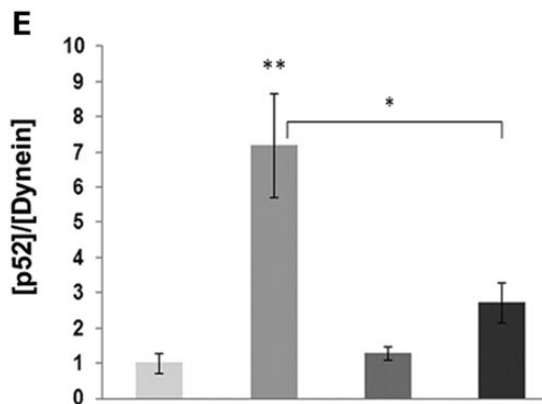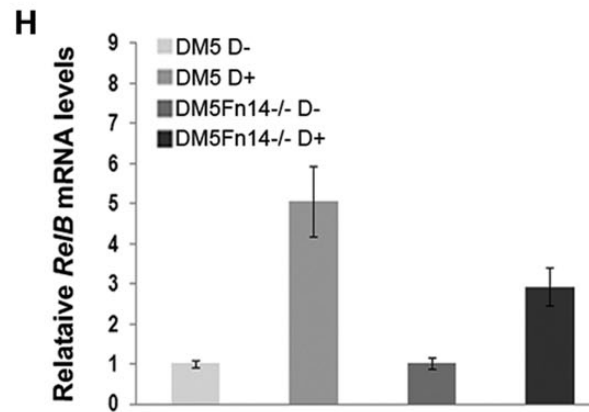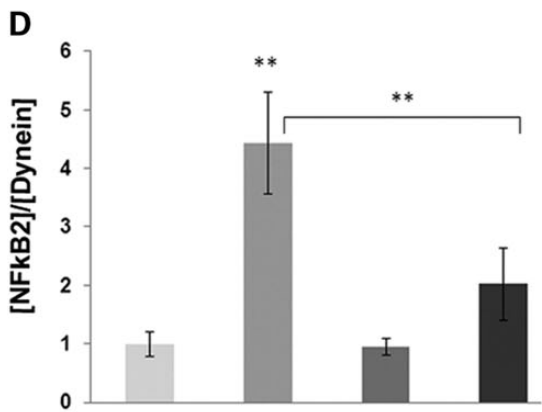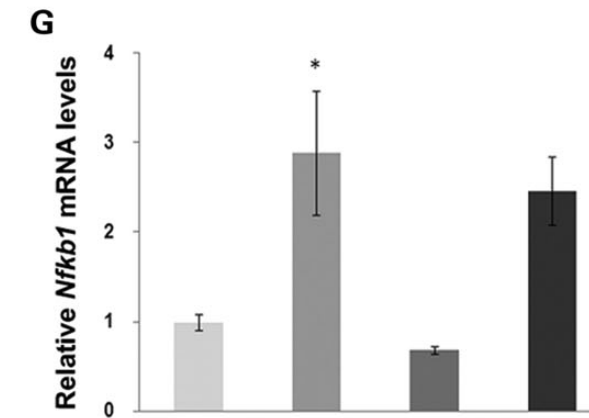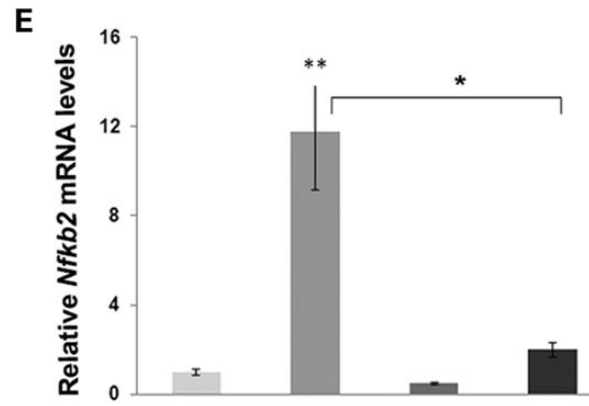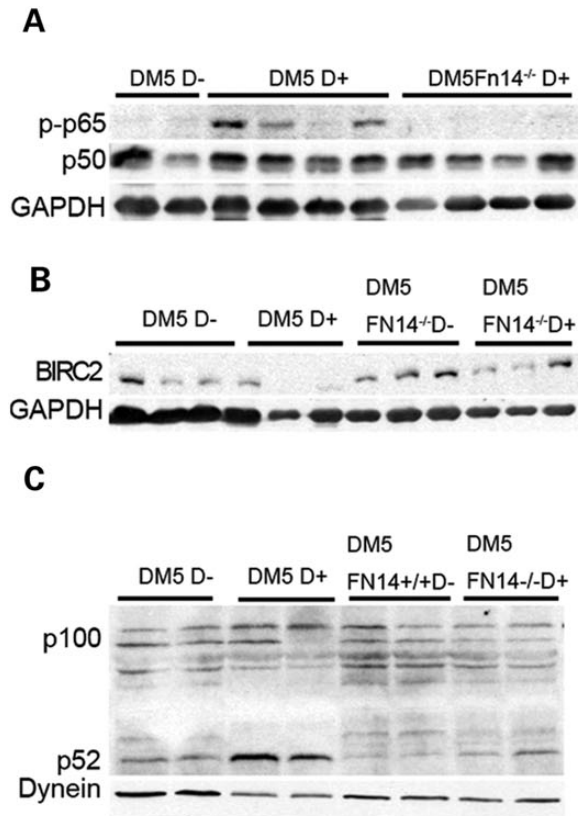
muscle histology in the P2D10 treated mice as compared with PBS or P1.17 treated mice (Fig. 8B and Supplementary Material, Fig. S12A). This was very similar to what was seen in DM5/$Fn14^{-/-}$-(D+) mice (Fig. 3C and Supplementary Material, Fig. S3D). Anti-TWEAK treatment trended towards improved grip strength ($P = 0.108$) and significantly better preservation of distance run ($P = 0.038$) (Fig. 8C and D). The previous experiments involved pre-dosing the mice prior to RNA toxicity. Since patients with DM1 typically present after disease onset, we induced RNA toxicity for 4 days in homozygous DM5 mice, a time when Fn14 is just being up-regulated in skeletal muscles (Fig. 1I), and then began treating with either P2D10 or P1.17. Though the mice received only three doses, there was still a strong trend towards significant benefit in grip strength ($P = 0.07$) (Supplementary Material, Fig. S12C), and a trend towards better treadmill running (Supplementary Material, Fig. S12C). Notably, DM5-(D+) mice treated with P2D10 also exhibited a clear trend towards increased cIAP1 levels ($P = 0.15$) (Supplementary Material, Fig. S13), and showed decreased expression of *Nfkb2* ($P = 0.057$) and *RelB* ($P = 0.063$) (Fig. 8E).

Of note, we have recently begun testing the therapy in an independent model of RNA toxicity. Given the cost of the therapeutics, a limited cohort of DM200 mice (aged 2 months) were induced with doxycycline for three weeks, underwent baseline phenotypic analyses (at which point they all had myotonia and mild cardiac conduction defects) and then treated with either

P2D10 ($n = 21$) or P1.17 ($n = 19$) given twice a week for 12 weeks. qRT-PCR confirmed no differences in the levels of toxic RNA between groups (Supplementary Material, Fig. S14). Though histopathology was noticeably milder in the DM200-(D+) mice as compared with the DM5-(D+) mice, there was still significant improvement in the P2D10 treated group (Fig. 8F). We found a significant difference in grip strength as early as 4 weeks after therapy ($P = 0.05$) and a significant difference ($P = 0.02$) at 10 weeks after therapy (Fig. 8G). Importantly, the P2D10 treated mice preserved their grip strength throughout as opposed to the P1.17 treated mice. Also, as seen in the treated DM5-(D+) mice, the P2D10 treated DM200-(D+) mice showed decreased expression of *Nfkb2* ($P = 0.04$), and *RelB* ($P = 0.075$) (Fig. 8H). No clear changes were seen in treadmill run performance at 10 weeks in the P2D10 cohort, though this might be skewed by the relatively better cardiac status of the few survivors in the group treated with the isotype control. Notably, by 12 weeks, we observed a trend towards decreased demise from P2D10 treatment with only a 38% mortality as compared with 70% mortality in the P1.17 group ($P = 0.089$, Mantel–Cox) (Fig. 8I).

Discussion

The investigation of DM1 pathogenesis and therapeutics development has almost exclusively focused on RNA splicing defects caused by the toxic RNA. We investigated whether additional

disease promoting mechanisms induced by RNA toxicity might contribute to DM1. Here we identify robust and physiologically important up-regulation of Fn14 and the TWEAK/Fn14 signaling pathway in skeletal muscles from individuals with DM1 and in mouse models of myotonic dystrophy. Though splicing defects are common in DM1, evaluation of *Fn14* splicing did not reveal any differences in any of our mouse models or in human tissues. We also show for the first time, significant activation of the canonical and non-canonical NF-κB pathways in skeletal muscles of DM1 individuals and in our mouse models of RNA toxicity, providing new potential targets for therapeutic intervention. Of note, inhibition of TWEAK/Fn14 signaling through genetic loss of *Fn14* or with a therapeutic molecule (anti-TWEAK antibody) results in significantly better performance outcomes and diminished muscle damage.

In healthy tissue, including skeletal muscle, Fn14 is expressed at very low levels, and is thought to be the limiting component of the TWEAK/Fn14 axis (24). However, Fn14 can be highly induced in states of tissue damage and chronic inflammation (24,34). Increasing evidence suggests that persistent TWEAK/Fn14 signaling plays an important and pathologic role in a number of clinical situations including chronic inflammatory diseases, stroke, and cardiac disease (16,24,35). Current models suggest that the acute activation of the TWEAK/Fn14 pathway via local inflammatory responses may promote early proliferative efforts in the muscle, but that prolonged activation in chronic disease leads to pathologic remodeling and tissue damage (24,36). Others have investigated the TWEAK/Fn14 pathway in skeletal muscle using cell culture or mouse models of artificially induced muscle damage (23). Chronic administration of TWEAK or transgenic over-expression in mice leads to activation of the ubiquitin/proteosome system, NF-κB activation, muscle atrophy, fibrosis and increased type II fibers in skeletal muscle, as well as impaired regeneration in response to induced damage (37–39). More recently, it has also been shown that TWEAK/Fn14 can also adversely affect metabolic pathways and expression of genes such as peroxisome proliferator-activated receptor γ coactivator 1α (PGC-1α) (29,40). Conversely, genetic ablation of TWEAK protects skeletal muscle after induced damage (38,39). This is akin to the protection afforded by *Fn14* deletion in the DM5 mice with RNA toxicity (Fig. 3). Likewise, cultured myoblasts and myotubes incubated with soluble TWEAK exhibit differentiation defects and myotube degeneration that is reversed by administering anti-TWEAK antibodies (37). A similar effect on preservation of muscle architecture is seen in the RNA toxicity mice treated with anti-TWEAK antibodies (Fig. 8 and Supplementary Material, Fig. S12A).

Fn14 induction is not a certainty in all muscle damage, and there was no clear prior evidence for the involvement of TWEAK/Fn14 in human muscular dystrophies (24). It is still unknown exactly how DM1 skeletal muscle pathology comes about other than the fact that it is associated with the expression of the toxic RNA. Many effects of increased TWEAK/Fn14 activity, including fibrosis, atrophic fibers, relative increase in type II fibers and a lack of a significant regenerative response, are all features of DM1 muscle pathology. Also, a number of mechanisms have been previously proposed in DM1 including defects in

regeneration, autophagy, inflammatory pathways, increased ubiquitin proteasome activity, and activation of signaling pathways including increased PKC and GSK-3β activity (12). Interestingly, many of these have also been implicated in the adverse effects of increased TWEAK/Fn14 signaling in skeletal muscle (29). Our results using RNA expression markers also show that RNA toxicity affects many of these pathways in our mouse model (Fig. 6 and Supplementary Material, Fig. S11). Notably, we also found evidence for potential beneficial effects of Fn14 deficiency in RNA toxicity, where the markers for inflammation (*Ccl-2* and *Ccl21a*) were reduced, while markers for autophagy (*Maplc3a* and *Maplc3b*), muscle metabolism (*Pgc1-α* and *Pgc1-β*) and regeneration (*Myh8*) were increased (Fig. 6 and Supplementary Material, Fig. S11). These results are consistent with existing ideas for other muscular dystrophies such as Duchenne muscular dystrophy where the increased inflammation and decreased regeneration have been therapeutic targets for years, and recent work in other mouse models of muscular dystrophy, where it has been shown that increases in autophagy and *Pgc1-α* expression can enhance muscle integrity and function (41–43). In addition, our results from the CTX experiments identified that RNA toxicity caused defects in satellite cell recruitment and expansion that were remedied by Fn14 deficiency (Fig. 7). All of these results support the notion that blocking Fn14 activity works through several pathways to improve muscle function and histopathology.

How Fn14 expression is up-regulated by RNA toxicity in DM1 is unclear. *In silico* analyses of the 5′ regions of both the mouse and human genes for Fn14 reveal a number of binding sites for transcription factors including NFκB, MyoD, GATA, SP1 and AP1. Signaling via TWEAK/Fn14 itself could have a positive feedback effect on Fn14 since this increased NFκB. In this regard, we observed that treatment of C2C12 myotubes with TWEAK increased levels of Fn14 in conjunction with increased signaling through the NFκB pathways (Supplementary Material, Fig. S5).

Given the remarkable clinical variability of DM1, many of the molecular changes in DM1 are also likely quite variable especially those tied to varying degrees of muscle degeneration. Thus, the significant correlation between Fn14 expression and its immediate downstream effects on NFκB pathways in both the mouse models and in tissues from DM1 patients is surprising and reassuring. As well, there seems to be a trend towards less demise with FN14 deficiency or anti-TWEAK treatment in mice with RNA toxicity. This is likely due to the beneficial effects of decreased TWEAK/Fn14 signaling on cardiac function. Increased Fn14 expression has been associated with adverse outcomes in mouse models of cardiac disease (35). Clearly, targeting the TWEAK/Fn14 pathway does not 'cure' DM1 in our mice. But, it does provide significant functional benefits which are laudable therapeutic goals. Targeting the toxic RNA may be the best approach to treating DM1. However, as in most clinical situations, a multi-pronged approach targeting various aspects of the disease often provides clear benefits to patients. It is becoming clear that DM1 pathology is likely to be multifactorial and a complicated picture, involving a number of mechanisms that contribute variably to the many facets of the disease phenotype (12). This is in

Figure 5. Deficiencies of FN14 attenuate NF-κB activation in mice with RNA toxicity. (**A–C**) Western blots of mouse skeletal muscle protein extracts show reduced levels of p-p65 (A), increased BIRC2 (B) and reduced NF-κB2 (p100 and p52) in DM5*Fn14*$^{-/-}$-(D+) mice (C). (**D** and **E**) Quantitative analysis of total NF-κB2 and p52 shows increased NF-κB2 and p52 in DM5-(D+) mice and reduced NF-κB2 and p52 in induced DM5*Fn14*$^{-/-}$ mice; ($n = 4$ mice per group), *$P = 0.03$, **$P = 0.004$ to 0.007. (**F–I**) qRT-PCR shows increased expression of *Nfkb2, Nfkb1, RelB* and *Map3k14 (Nik)* in DM5-(D+) mice and significant reductions in *Nfkb2* (F) and *Map3k14* (I) expression in DM5*Fn14*$^{-/-}$-(D+) mice; $n ≥ 5$ per group; error bars are mean ± SEM; *$P = 0.01$ to 0.03, **$P = 0.002$ to 0.003, ***$P = 0.0007$ (Student's t test).
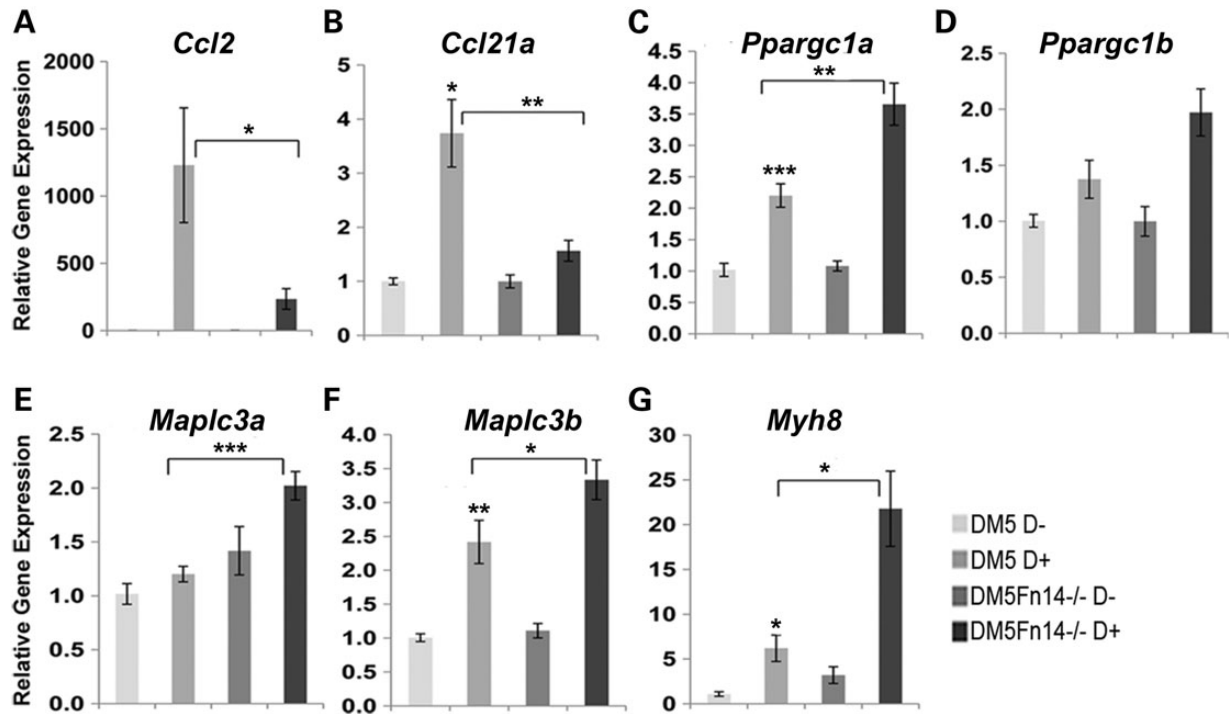
Figure 6. Effects of Fn14 deficiency on downstream pathways implicated in RNA toxicity and TWEAK/Fn14 pathology in skeletal muscle. (**A** and **B**) RNA toxicity (DM5-(D+) in skeletal muscle is associated with increased expression of inflammatory cytokines (*Ccl2* and *Ccl21a*) and Fn14 deficiency significantly dampens this effect. (**C** and **D**) Fn14 deficiency significantly improves *Pgc-1α* (Ppargc1a) expression in mice with RNA toxicity. (**E** and **F**) *Maplc3a* and *Maplc3b* both show significant increased expression in DM5-(D+) mice with Fn14 deficiency. (**G**) *Myh8* expression is significantly increased in the skeletal muscle of RNA toxicity mice lacking Fn14, suggesting an improved regenerative response. All these changes correlate with the improved histopathology seen in these mice (see Supplementary Material, Fig. S3D). $n = 5$–10 per group; (*$P = 0.02$–0.05, **$P = 0.003$–0.007, ***$P = 0.0002$–0.0003, Student's t test); error bars are mean ± SEM.
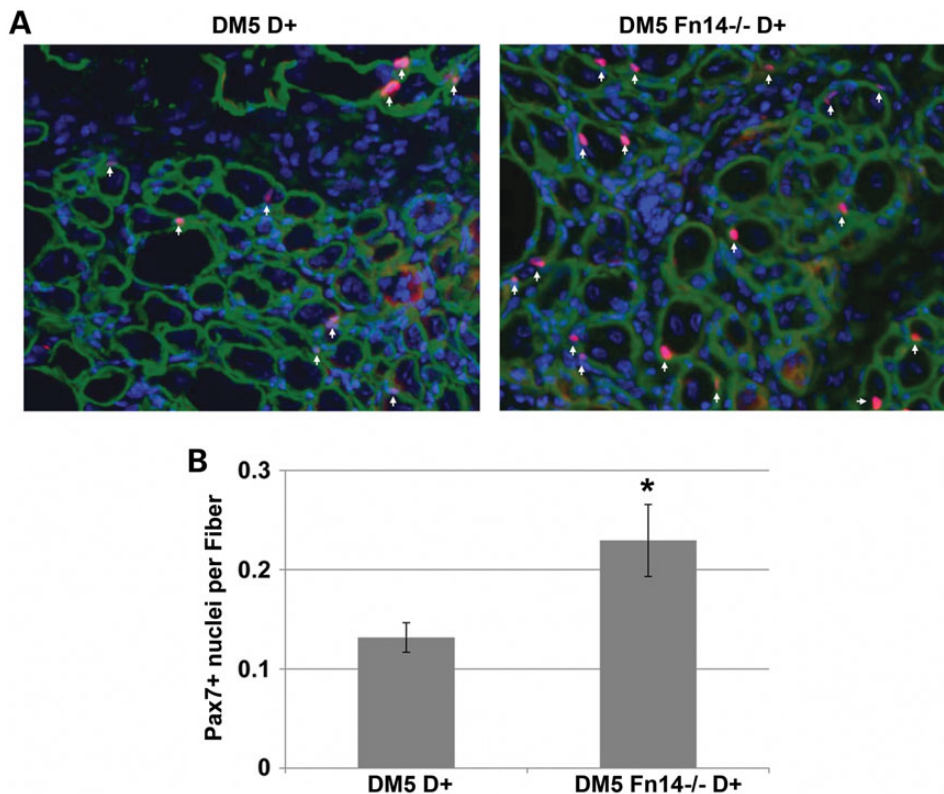

Figure 7. Fn14 deficiency corrects satellite cell response defects in mice with RNA toxicity. (**A**) Representative PAX7 immunofluorescence images of skeletal muscle sections 5 days after CTX damage (arrowheads indicate PAX7+ve nuclei). PAX7 (red); Laminin (green); nuclei (blue); genotypes of mice as indicated. (**B**) Quantification of Pax7 positive nuclei per myofiber shows that the number of PAX7+nuclei is increased by Fn14 deficiency. Data presented as mean ± SD; $n = 3$–5 per group; *$P = 0.02$ (Mann–Whitney).
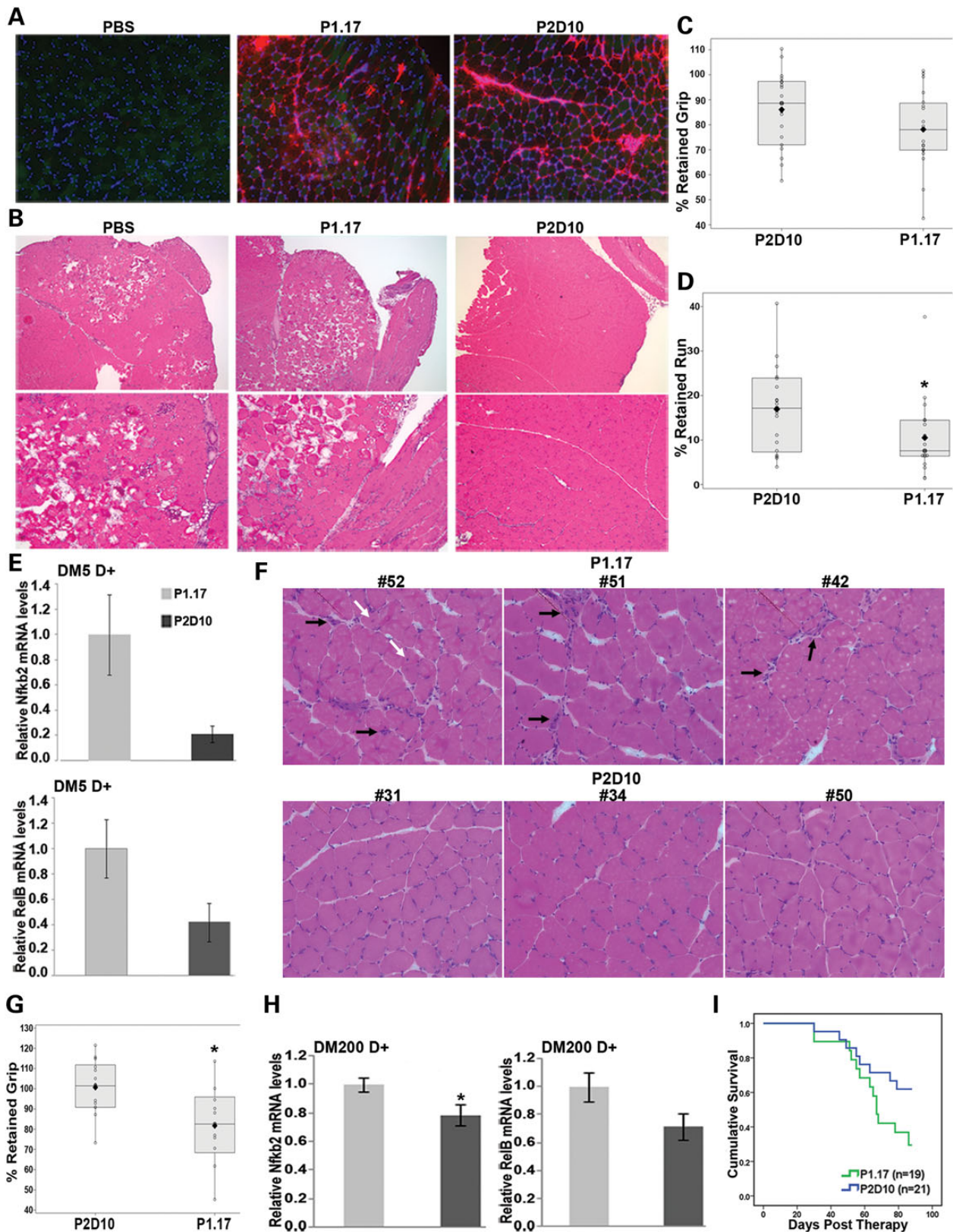
Figure 8. Anti-TWEAK antibody therapy leads to improved outcomes. (**A**) Indirect immunofluorescence (red) using an anti-IgG2a antibody shows that P1.17 and P2D10 are present in muscle fibers of treated mice. (**B**) H&E stained muscle sections show that P2D10 treated DM5-(D+) mice have less degeneration and better preserved muscle than mice treated with PBS or P1.17; ×40 and ×100 magnification. (**C** and **D**) At 14 days post-induction, P2D10 treated mice demonstrated a trend towards preservation of grip strength ($P = 0.108$) and a significant preservation of run ability (*$P = 0.038$); ($n = 18$ to 20 per group); Student's *t* test. See Fig. 2I legend for description of graphical markings. (**E**) qRT-PCR of *Nfkb2*, *RelB*, expression in DM5-(D+) mice treated with P2D10 versus P1.17. ($n \geq 6$ per group); $P = 0.057$ for *Nfkb2*, $P = 0.063$ for *RelB*; Student's *t* test. (**F**) The top

some ways a therapeutic opportunity, as it provides multiple potential avenues to intervene in the disease.

In summary, we identified induced Fn14 and increased TWEAK/Fn14 signaling as a novel molecular pathogenic mechanism caused by RNA toxicity in DM1. This led us to test the hypothesis that blocking this pathway may be of clinical benefit. Our results support the potential for using anti-TWEAK to treat key aspects of DM1 pathology, either alone or perhaps in a combinatorial approach with other therapies under development. Of note, our data suggest that evidence of significant clinical weakness by manual muscle testing in individuals with DM1 might be a simple but effective tool in selecting patients for a potential clinical trial, as it seems like a very good predictor of increased *FN14* expression in their skeletal muscles (Fig. 2G). An anti-TWEAK antibody (BIIB023) is currently being studied in Phase II clinical trials in patients with rheumatoid arthritis and lupus nephritis and has thus far displayed an excellent safety profile (44). Our results in conjunction with the development of BIIB023 offer the promise of the first available therapeutic to modify progression of muscle damage and muscle dysfunction, issues that currently cause significant disability and deterioration in quality of life in DM1 patients.

Materials and Methods

Transgenic mice

Transgenic design and phenotypic characterization of DM5, DM200, $Fn14^{-/-}$ and $TWEAK^{-/-}$ transgenic mice are described elsewhere (5,19,45). The DM5 line expresses an eGFP-*DMPK* 3′ UTR (CTG)$_5$ transgene under the control of a doxycycline responsive human *DMPK* promoter. Induced DM5 mice typically develop phenotypes within 3–5 days and die within 2–3 weeks usually from cardiac conduction abnormalities and cardiac failure (5,14). The DM200 line is similar except that it expresses an eGFP-*DMPK* 3′UTR (CTG)$_{200}$ transgene. The mice are normal prior to transgene induction. Transgenic mice were induced with 0.2% doxycycline in drinking water. The DM5 mice are in an FVB background. The DM200s are in a FVB/Bl6 mixed background. All experiments using the DM5/$Fn14^{-/-}$ or DM5/$Tweak^{-/-}$ mice were done with littermate controls that were generated through the breeding process.

Human skeletal muscle samples

Skeletal muscle samples used for most of the experiments were from autopsy cases. Anonymous DM1 muscle samples ($n = 8$) were provided by Dr Thornton. Samples (with equal gender representation) were either from biceps or quadriceps femoris of patients with classic adult onset DM1. Age range at death was from∼45–55. The size of the (CTG) expansion was not available. Unaffected samples from adults were obtained from tissue banks and autopsy cases. For the TA biopsy samples used in Figure 2G, adult subjects were recruited by Dr Thornton as part of an IRB approved protocol and clinically assessed using the MRC rating scale for standardized manual muscle testing (Supplementary Material, Table S3). The diagnosis in all individuals with DM1 was confirmed by molecular testing.

Treadmill running, forelimb grip strength, EMGs and ECGs

Protocols for treadmill running and grip strength, EMGs and ECGs are described elsewhere (5,46,47). Testers were blind to genotype. All protocols were approved by institutional committees for animal care and use. Twenty mice per study group (for the DM5 mice) were all assessed pre-induction (baseline), and all surviving mice at 14 days post-induction of RNA toxicity. All results were reported as retained function with reference to baseline for each mouse.

Histology and immunofluorescence microscopy

Tissues were collected in isopentane and flash frozen in liquid nitrogen. Serial cryostat sections (6 µm) of skeletal muscles (paraspinal or quadriceps femoris) were prepared. Hematoxylin and eosin (H&E) staining was done according to standard procedures and examined under a light microscope. Indirect immunofluorescence was performed after fixation using 4% paraformaldehyde (5). Primary antibodies were anti-FN14 (Epitomics®, #3488-1; 1:1000 dilution), anti-mouse IgG2a-Alexa594 (Invitrogen™ #A21135; 1:1000 dilution), anti-NIK (Cell Signaling Tech.® #4994; 1:200 dilution), anti-NFKB2 (Cell Signaling Tech.® #4882; 1:200 dilution). Secondary antibodies were from Molecular Probes™ (1:400–1:1000 dilution). Microscopy was performed using an Olympus IX 50 inverted microscope with fluorescent attachments and images were captured with a CCD camera.

Cardiotoxin injection and PAX7 immunofluorescence

DM5-313$^{+/+}$ and DM5-313$^{+/+}$ Fn14$^{-/-}$ mice were either kept on normal water (uninduced) or given 0.2% doxycycline (induced) for 7 days. After 7 days, the TA muscles in each mouse were injected with either 10 µM CTX or PBS. Indirect immunofluorescence for PAX7 was done with tissues collected 5 days after CTX injection. Flash frozen 6 µm sections were fixed with 4% paraformaldehyde. Primary antibodies were anti-PAX7 (DSHB, PAX7-c; 1:50 dilution), anti-laminin (Sigma, #L9393; 1:200 dilution). Secondary antibodies were from Molecular Probes™ (1:1000 dilutions).

Muscle-fiber size determination

Muscle fiber size was determined by measuring cross-sectional area of each muscle fiber in a ×200 image of H&E stained skeletal muscle. Three to five mice per group were analyzed, and for each mouse at least three different images and at least 300 fibers were analyzed. Muscle fiber size was measured using AxioVision™ V4.8.2.0 (Carl Zeiss MicroImaging).

Histopathology grading scale

The grading scale was based on criteria used in clinical practice by neuropathologists. Three to five visual fields (at ×200) were scored for (1) the percentage of central nuclei, (2) evidence of inflammation, (3) percentage of atrophic fibers, (4) evidence of significant fibre size variability and (5) the presence or absence of fibrosis. Each criterion was scored on a scale (0–3) and the total

row shows three examples of H&E stained skeletal muscle from DM200-(D+) mice treated with P1.1.7. Muscle fibers have numerous central nuclei (white arrows), nuclear clumping with atrophic fibers (black arrows) and exhibit fiber degeneration resulting in fiber size variation. The bottom row shows three examples of H&E stained skeletal muscle from induced mice treated with P2D10. Note clear benefit in muscle histology in P2D10 treated mice. Histopathology grading confirmed significant differences ($P = 0.03$, Mann–Whitney) ($n = 5$ per group; 500–600 fibers per mouse). All pictures, ×200 magnification. (**G**) P2D10 treated DM200-(D+) mice have preserved grip strength (101 versus 82% at 10 weeks), **$P = 0.02$ (Mann–Whitney). See Fig. 2I legend for description of graphical markings. (**H**) qRT-PCR of *Nfkb2*, *RelB*, expression in DM200-(D+) mice treated with P2D10 versus P1.17. ($n = 5$ per group); *$P = 0.04$ for *Nfkb2*, $P = 0.075$ for *RelB*. Error bars are mean ± SEM (Student's t test). (**I**) Kaplan–Meier curve shows decreased demise in P2D10 treated DM200-(D+) mice ($P = 0.089$, Mantel–Cox).

score was used to for a histopathology grade (Supplementary Material, Table S1).

Northern blot analysis

Total RNA was extracted from flash frozen tissues. Northern blots of 5–10 µg of total RNAs separated on 1% glyoxal gels were probed with *Fn14* or glyceraldehyde phosphate dehydrogenase (*Gapdh*) cDNAs using standard procedures.

qRT-PCR assays

RNAs were treated with DNAseI (Ambion®, cat.# 1907) and then cDNAs were synthesized using the QuantiTect™ Reverse Transcription Kit (Qiagen®, Cat. No. #20531). The cDNAs from the TA biopsies were generated using a NuGEN® Ovation® RNA-Seq System. qRT-PCR was done using the BioRad iCycler™ and detected with SYBRGreen™ dye. All assays were done in duplicate, and the data were normalized to an endogenous control (*Gapdh*). The values were subjected to a $2^{(-\Delta\Delta Ct)}$ formula to calculate the fold change between the control and experimental groups. Fold change post-induction was calculated relative to appropriate un-induced genetically identical mice. For primer sequences, PCR conditions and efficiency, see Supplementary Material, Table S4.

Western blotting

Total protein extracts from frozen tissues were made using standard protocols in RIPA buffer [50 mM Tris–HCl, pH 7.4, 150 mM NaCl, 1% NP40, 0.5% Na-deoxycholate, 0.1% sodium dodecyl sulfate (SDS)] and protease inhibitor (Roche Inc., cat.# 1873580). To detect murine and human protein, 50 µg of skeletal muscle extracts were loaded onto a 12% SDS-polyacrylamide gel electrophoresis gel. The blot was blocked in PBS with 5% milk for 1 h then incubated overnight at 4°C in PBS with 5% milk with primary antibody. GAPDH, dyenin or tubulin were used as loading controls. Blots were scanned and relative protein expression was quantified using Image Quant5.1™. The following antibodies were used; for mouse proteins: Fn14 (Epitomics® #3488–1), GAPDH (Ambion® #4300), Tubulin (Sigma-Aldrich® #T6199), Dynein (Santa Cruz Biotech, Inc. #SC-13524), anti-mouse IgG2a-HRP (Invitrogen™ #M32307), Ciap1(BIRC2) (R&D® #MAB3400), NFκB2(p100 and p52) (Cell Signaling Tech.® #4882), NFκB1(p50) (Epitomics® #1559-1), NIK (Cell Signaling Tech.® #4994), p-p65 Ser-536 (Cell Signaling Tech.® #3031). For human proteins: Fn14 (Epitomics® #3488-1), cIAP (BIRC2) (Enzo® 1E-1-10), p-p65 Ser-536 (Cell Signaling Tech.® #3031), NFκB2 (p100 and p52) (Millipore© #05-361), NFκB1 (Cell Signaling Tech.® #3035), GAPDH (Ambion® #4300), Tubulin (Sigma-Aldrich® #T6199).

Anti-TWEAK antibody (P2D10)

Generation of the monoclonal P2D10 antibody is described elsewhere ([36](#)). Briefly, *Tweak*$^{-/-}$ mice were exposed to TWEAK ligand at defined intervals, and affinity purification methods were used to obtain monoclonal antibody stocks from inoculated mice. Intraperitoneal injections of either P2D10 antibody, isotype control (P1.17), both at 30 µg/g of body weight), or PBS (200 µl) were given every 3 days as suggested by Biogen Idec based on their in-house studies.

Statistical analysis

Standard statistical methods were employed. Briefly, data sets were first analyzed for outliers using the Grubb's test, also known as the ESD method (extreme studentized deviate). For real-time PCR, outliers were assessed prior to calculation of fold change. Once outliers were removed, the data set was analyzed

for normality. If normal, two-tailed Student's *T*-tests were employed to assess significance, with attention paid to equal versus unequal variance. ANOVA analysis (Tukey multiple comparison) was used for Figure [2](#)I. If the data set was non-normal, the Mann–Whitney assessment for statistical significance was used. Kaplan–Meier curve analysis with the Mantel–Cox test were also used as indicated. Minitab® 16.1.0 (Minitab, Inc.) was the software used.

Study approvals

All animal protocols (# 3218) were approved by the institutional ICAUC at the University of Virginia. All anonymous samples provided by Dr Thornton were collected under an University of Rochester IRB approved protocol (# 247921) which included a written informed consent from all participants prior to inclusion in the study.

Supplementary Material

Supplementary Material is available at *HMG* online.

Authors' Contributions

M.S.M. discovered Fn14 induction in RNA toxicity mice, did microscopy, phenotyping, evaluation of therapeutics, experimental design and wrote the manuscript. R.S.Y co-wrote the manuscript, and did experimental design and all experiments on downstream signaling. E.P.F. co-wrote the manuscript, designed and did phenotyping and tested therapeutics in concert with Q.Y. and M.S.M. J.T.G. did expression analyses, statistical analyses, histopathology grading and PAX7 studies. Y.K.K. graded histopathology. K.B. and C.A.T. provided anonymous cDNA samples and information on the cohort of clinically evaluated individuals. T.Z. helped design experiments and provided reagents.

Conflict of Interest statement. T.Z. is an employee and stockholder of Biogen Idec.

Funding

References

1. Turner, C. and Hilton-Jones, D. (2010) The myotonic dystrophies: diagnosis and management. *J. Neurol. Neurosurg. Psychiatry*, **81**, 358–367.
2. Amack, J.D., Paguio, A.P. and Mahadevan, M.S. (1999) *Cis* and *trans* effects of the myotonic dystrophy (DM) mutation in a cell culture model. *Hum. Mol. Genet.*, **8**, 1975–1984.
3. Mahadevan, M., Tsilfidis, C., Sabourin, L., Shutler, G., Amemiya, C., Jansen, G., Neville, C., Narang, M., Barcelo, J., O'Hoy, K. *et al.* (1992) Myotonic dystrophy mutation: an unstable CTG repeat in the 3′ untranslated region of the gene. *Science*, **255**, 1253–1255.
4. Taneja, K.L., McCurrach, M., Schalling, M., Housman, D. and Singer, R.H. (1995) Foci of trinucleotide repeat transcripts in

nuclei of myotonic dystrophy cells and tissues. *J. Cell Biol.*, **128**, 995–1002.

5. Mahadevan, M.S., Yadava, R.S., Yu, Q., Balijepalli, S., Frenzel-McCardell, C.D., Bourne, T.D. and Phillips, L.H. (2006) Reversible model of RNA toxicity and cardiac conduction defects in myotonic dystrophy. *Nat. Genet.*, **38**, 1066–1070.

6. Mankodi, A., Logigian, E., Callahan, L., McClain, C., White, R., Henderson, D., Krym, M. and Thornton, C.A. (2000) Myotonic dystrophy in transgenic mice expressing an expanded CUG repeat. *Science*, **289**, 1769–1773.

7. Echeverria, G.V. and Cooper, T.A. (2012) RNA-binding proteins in microsatellite expansion disorders: mediators of RNA toxicity. *Brain Res.*, **1462**, 100–111.

8. Childs-Disney, J.L., Hoskins, J., Rzuczek, S.G., Thornton, C.A. and Disney, M.D. (2012) Rationally designed small molecules targeting the RNA that causes myotonic dystrophy type 1 are potently bioactive. *ACS Chem. Biol.*, **7**, 856–862.

9. Warf, M.B., Nakamori, M., Matthys, C.M., Thornton, C.A. and Berglund, J.A. (2009) Pentamidine reverses the splicing defects associated with myotonic dystrophy. *Proc. Natl. Acad. Sci. U S A*, **106**, 18551–18556.

10. Wheeler, T.M., Leger, A.J., Pandey, S.K., MacLeod, A.R., Nakamori, M., Cheng, S.H., Wentworth, B.M., Bennett, C.F. and Thornton, C.A. (2012) Targeting nuclear RNA for in vivo correction of myotonic dystrophy. *Nature*, **488**, 111–115.

11. Jones, K., Wei, C., Iakova, P., Bugiardini, E., Schneider-Gold, C., Meola, G., Woodgett, J., Killian, J., Timchenko, N.A. and Timchenko, L.T. (2012) GSK3beta mediates muscle pathology in myotonic dystrophy. *J. Clin. Invest.*, **122**, 4461–4472.

12. Mahadevan, M.S. (2012) Myotonic dystrophy: is a narrow focus obscuring the rest of the field? *Curr. Opin. Neurol.*, **25**, 609–613.

13. Rau, F., Freyermuth, F., Fugier, C., Villemin, J.P., Fischer, M.C., Jost, B., Dembele, D., Gourdon, G., Nicole, A., Duboc, D. *et al.* (2011) Misregulation of miR-1 processing is associated with heart defects in myotonic dystrophy. *Nat. Struct. Mol. Biol.*, **18**, 840–845.

14. Yadava, R.S., Frenzel-McCardell, C.D., Yu, Q., Srinivasan, V., Tucker, A.L., Puymirat, J., Thornton, C.A., Prall, O.W., Harvey, R.P. and Mahadevan, M.S. (2008) RNA toxicity in myotonic muscular dystrophy induces NKX2-5 expression. *Nat. Genet.*, **40**, 61–68.

15. Wiley, S.R., Cassiano, L., Lofton, T., Davis-Smith, T., Winkles, J.A., Lindner, V., Liu, H., Daniel, T.O., Smith, C.A. and Fanslow, W.C. (2001) A novel TNF receptor family member binds TWEAK and is implicated in angiogenesis. *Immunity*, **15**, 837–846.

16. Burkly, L.C., Michaelson, J.S., Hahm, K., Jakubowski, A. and Zheng, T.S. (2007) TWEAKing tissue remodeling by a multifunctional cytokine: role of TWEAK/Fn14 pathway in health and disease. *Cytokine*, **40**, 1–16.

17. Chicheportiche, Y., Bourdon, P.R., Xu, H., Hsu, Y.M., Scott, H., Hession, C., Garcia, I. and Browning, J.L. (1997) TWEAK, a new secreted ligand in the tumor necrosis factor family that weakly induces apoptosis. *J. Biol. Chem.*, **272**, 32401–32410.

18. Brown, S.A., Cheng, E., Williams, M.S. and Winkles, J.A. (2013) TWEAK-independent Fn14 self-association and NF-kappaB activation is mediated by the C-terminal region of the Fn14 cytoplasmic domain. *PLoS One*, **8**, e65248.

19. Girgenrath, M., Weng, S., Kostek, C.A., Browning, B., Wang, M., Brown, S.A., Winkles, J.A., Michaelson, J.S., Allaire, N., Schneider, P. *et al.* (2006) TWEAK, via its receptor Fn14, is a novel regulator of mesenchymal progenitor cells and skeletal muscle regeneration. *EMBO J.*, **25**, 5826–5839.

20. Brown, S.A., Richards, C.M., Hanscom, H.N., Feng, S.L. and Winkles, J.A. (2003) The Fn14 cytoplasmic tail binds tumour-necrosis-factor-receptor-associated factors 1, 2, 3 and 5 and mediates nuclear factor-kappaB activation. *Biochem. J.*, **371**, 395–403.

21. Kumar, M., Makonchuk, D.Y., Li, H., Mittal, A. and Kumar, A. (2009) TNF-like weak inducer of apoptosis (TWEAK) activates proinflammatory signaling pathways and gene expression through the activation of TGF-beta-activated kinase 1. *J. Immunol.*, **182**, 2439–2448.

22. Roos, C., Wicovsky, A., Muller, N., Salzmann, S., Rosenthal, T., Kalthoff, H., Trauzold, A., Seher, A., Henkler, F., Kneitz, C. *et al.* (2010) Soluble and transmembrane TNF-like weak inducer of apoptosis differentially activate the classical and noncanonical NF-kappa B pathway. *J. Immunol.*, **185**, 1593–1605.

23. Bhatnagar, S. and Kumar, A. (2012) The TWEAK-Fn14 system: breaking the silence of cytokine-induced skeletal muscle wasting. *Curr. Mol. Med.*, **12**, 3–13.

24. Burkly, L.C., Michaelson, J.S. and Zheng, T.S. (2011) TWEAK/Fn14 pathway: an immunological switch for shaping tissue responses. *Immunol. Rev.*, **244**, 99–114.

25. Sanz, A.B., Sanchez-Nino, M.D., Izquierdo, M.C., Jakubowski, A., Justo, P., Blanco-Colio, L.M., Ruiz-Ortega, M., Selgas, R., Egido, J. and Ortiz, A. (2010) TWEAK activates the non-canonical NFkappaB pathway in murine renal tubular cells: modulation of CCL21. *PLoS One*, **5**, e8955.

26. Bakkar, N. and Guttridge, D.C. (2010) NF-kappaB signaling: a tale of two pathways in skeletal myogenesis. *Physiol. Rev.*, **90**, 495–511.

27. Shin, J., Tajrishi, M.M., Ogura, Y. and Kumar, A. (2013) Wasting mechanisms in muscular dystrophy. *Int. J. Biochem. Cell. Biol.*, **10**, 2266–2279.

28. Leeman, J.R. and Gilmore, T.D. (2008) Alternative splicing in the NF-kappaB signaling pathway. *Gene*, **423**, 97–107.

29. Sato, S., Ogura, Y. and Kumar, A. (2014) TWEAK/Fn14 signaling axis mediates skeletal muscle atrophy and metabolic dysfunction. *Front. Immunol.*, **5**, 18.

30. Ogura, Y., Mishra, V., Hindi, S.M., Kuang, S. and Kumar, A. (2013) Proinflammatory cytokine tumor necrosis factor (TNF)-like weak inducer of apoptosis (TWEAK) suppresses satellite cell self-renewal through inversely modulating Notch and NF-kappaB signaling pathways. *J. Biol. Chem.*, **288**, 35159–35169.

31. Gladman, J.T., Yadava, R.S., Mandal, M., Yu, Q., Kim, Y.K. and Mahadevan, M.S. (2015) NKX2-5, a modifier of skeletal muscle pathology due to RNA toxicity. *Hum. Mol. Genet.*, **24**, 251–264.

32. Bentzinger, C.F., Wang, Y.X., Dumont, N.A. and Rudnicki, M.A. (2013) Cellular dynamics in the muscle satellite cell niche. *EMBO Rep.*, **14**, 1062–1072.

33. Michaelson, J.S., Wisniacki, N., Burkly, L.C. and Putterman, C. (2012) Role of TWEAK in lupus nephritis: a bench-to-bedside review. *J. Autoimmun.*, **39**, 130–142.

34. Winkles, J.A. (2008) The TWEAK-Fn14 cytokine-receptor axis: discovery, biology and therapeutic targeting. *Nat. Rev. Drug. Discov.*, **7**, 411–425.

35. Ren, M.Y. and Sui, S.J. (2012) The role of TWEAK/Fn14 in cardiac remodeling. *Mol. Biol. Rep.*, **39**, 9971–9977.

36. Morosetti, R., Gliubizzi, C., Sancricca, C., Broccolini, A., Gidaro, T., Lucchini, M. and Mirabella, M. (2012) TWEAK in inclusion-body myositis muscle: possible pathogenic role of a cytokine inhibiting myogenesis. *Am. J. Pathol.*, **180**, 1603–1613.

37. Dogra, C., Changotra, H., Wedhas, N., Qin, X., Wergedal, J.E. and Kumar, A. (2007) TNF-related weak inducer of apoptosis (TWEAK) is a potent skeletal muscle-wasting cytokine. *FASEB J.*, **21**, 1857–1869.

38. Mittal, A., Bhatnagar, S., Kumar, A., Lach-Trifilieff, E., Wauters, S., Li, H., Makonchuk, D.Y., Glass, D.J. and Kumar, A. (2010) The TWEAK-Fn14 system is a critical regulator of denervation-induced skeletal muscle atrophy in mice. *J. Cell. Biol.*, **188**, 833–849.

39. Mittal, A., Bhatnagar, S., Kumar, A., Paul, P.K., Kuang, S. and Kumar, A. (2010) Genetic ablation of TWEAK augments regeneration and post-injury growth of skeletal muscle in mice. *Am. J. Pathol.*, **177**, 1732–1742.

40. Hindi, S.M., Mishra, V., Bhatnagar, S., Tajrishi, M.M., Ogura, Y., Yan, Z., Burkly, L.C., Zheng, T.S. and Kumar, A. (2014) Regulatory circuitry of TWEAK-Fn14 system and PGC-1alpha in skeletal muscle atrophy program. *FASEB J.*, **28**, 1398–1411.

41. De Palma, C., Morisi, F., Cheli, S., Pambianco, S., Cappello, V., Vezzoli, M., Rovere-Querini, P., Moggio, M., Ripolone, M., Francolini, M. *et al.* (2012) Autophagy as a new therapeutic target in Duchenne muscular dystrophy. *Cell Death Dis.*, **3**, e418.

42. Hollinger, K., Gardan-Salmon, D., Santana, C., Rice, D., Snella, E. and Selsby, J.T. (2013) Rescue of dystrophic skeletal muscle by PGC-1alpha involves restored expression of dystrophin-associated protein complex components and satellite cell signaling. *Am. J. Physiol. Regul. Integr. Comp. Physiol.*, **305**, R13–R23.

43. Selsby, J.T., Morine, K.J., Pendrak, K., Barton, E.R. and Sweeney, H.L. (2012) Rescue of dystrophic skeletal muscle by PGC-1alpha involves a fast to slow fiber type shift in the mdx mouse. *PLoS One*, **7**, e30063.

44. Wisniacki, N., Amaravadi, L., Galluppi, G.R., Zheng, T.S., Zhang, R., Kong, J. and Burkly, L.C. (2013) Safety, tolerability, pharmacokinetics, and pharmacodynamics of anti-TWEAK monoclonal antibody in patients with rheumatoid arthritis. *Clin. Ther.*, **35**, 1137–1149.

45. Campbell, S., Burkly, L.C., Gao, H.X., Berman, J.W., Su, L., Browning, B., Zheng, T., Schiffer, L., Michaelson, J.S. and Putterman, C. (2006) Proinflammatory effects of TWEAK/Fn14 interactions in glomerular mesangial cells. *J. Immunol.*, **176**, 1889–1898.

46. Gladman, J.T., Mandal, M., Srinivasan, V. and Mahadevan, M. S. (2013) Age of onset of RNA toxicity influences phenotypic severity: evidence from an inducible mouse model of myotonic dystrophy (DM1). *PLoS One*, **8**, e72907.

47. Kim, Y.K., Mandal, M., Yadava, R.S., Paillard, L. and Mahadevan, M.S. (2014) Evaluating the effects of CELF1 deficiency in a mouse model of RNA toxicity. *Hum. Mol. Genet.*, **23**, 293–302.